View metadata, citation and similar papers at core.ac.uk
brought to you by CORE
provided by Repositori Institucional de la Universitat Jaume I

ACS OMEGA
Article
Cite This: ACS Omega 2018, 3, 9798−9804
http://pubs.acs.org/journal/acsodf

Optical Optimization of the TiO_2 Mesoporous Layer in Perovskite Solar Cells by the Addition of SiO_2 Nanoparticles

Naemeh Aeineh,[†,‡] Andrés-Felipe Castro-Méndez,[§] Pedro J. Rodriguez-Cantó,[∥] Rafael Abargues,[⊥] Ehsan Hassanabadi,[†,#] Isaac Suarez,[†,⊥] Abbas Behjat,[‡] Pablo Ortiz,[§] Juan P. Martínez-Pastor,[∥] and Ivan Mora-Seró*[,†]

[†]Institute of Advanced Materials (INAM), Universitat Jaume I, Castelló 12006, Spain
[‡]Atomic and Molecular Group, Faculty of Physics, Yazd University, Yazd 51167-87317, Iran
[§]Grupo de Diseño de Productos y Procesos (GDPP), Chemical Engineering Department, Universidad de los Andes, Bogotá 111711, Colombia
[∥]Intenanomat S.L., C/Catedrático José Beltrán 2, 46980 Paterna, Spain
[⊥]UMDO, Instituto de Ciencia de los Materiales, Universidad de Valencia, Valencia 46071, Spain
[#]Textile Engineering Department, Textile Excellence & Research Centers, Amirkabir University of Technology, Hafez Avenue, Tehran 1591634311, Iran

Supporting Information

ABSTRACT: In this work, SiO_2 nanoparticles (NPs) were integrated into the mesoporous TiO_2 layer of a perovskite solar cell to investigate their effect on cell performance. Different concentrations of SiO_2/ethanol have been combined in TiO_2/ethanol to prepare pastes for the fabrication of the mesoporous layer with which perovskite solar cells have been fabricated. Addition of SiO_2 NPs of 50 and 100 nm sizes produces an enhancement of cell performance mainly because of an improvement of the photocurrent. This increment is in good agreement with the theoretical predictions based on light scattering induced by dielectric SiO_2 NPs. The samples using modified scaffolds with NPs also present a significant lower current−potential hysteresis indicating that NP incorporation also affects the ion accumulation at the perovskite interface, providing an additional beneficial effect. The results stress the importance of the appropriated management of the optical properties on further optimization of perovskite solar cell technology.

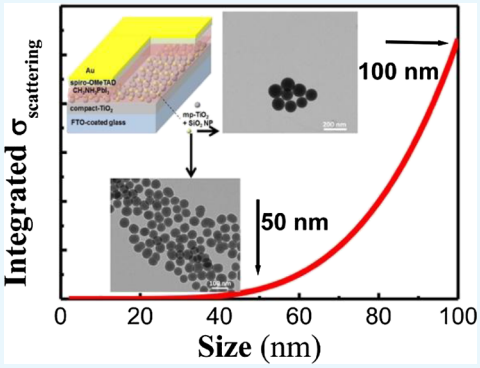

1. INTRODUCTION

Ever since the seminal reports in sensitized[1,2] and in all-solid solar cell configurations,[3,4] halide perovskites have been widely investigated as light harvesters in solar cells because of their optimal properties, including direct band gap, large absorption coefficients, and high carrier mobility.[5] Indeed, the significant work carried out in the research resulted in a power conversion efficiency (PCE) of perovskite solar cells (PSCs) close to 23%.[6] The main strategy to enhance PCE has been the optimization of the deposition process and of the halide perovskite harvester by the use of multication/anion perovskites.[7−11] However, other strategies have been employed including the incorporation of noble metal nanoparticles (NPs), increase of the thickness of the absorbing material, adding scattering layers, or the use of back reflectors and other light-trapping mechanisms.[12−14] In these cases, the improvement on solar cell performance is attained by the management of the optical properties of the device. For example, deposition of gold and silver NPs is a common approach because of their high (and size tuned) scattering and absorption cross-sections.[15] They have also been shelled with SiO_2[16−18] to protect them from the corrosive effect of iodine and incorporated in the architecture of PSCs, observing an enhancement of the device performance.[17] Theoretical studies predict that core−shell Au/SiO_2 NPs provide optical absorption enhancement in PSCs in spectral regions where the perovskite material has relatively poor absorption.[19−21] It is suggested that this enhancement is mainly based on a plasmonic effect, but it is not the only way in which Au/SiO_2 NPs can help to enhance the PSC performance. Recently, we have used Au/SiO_2 NPs with a smaller Au core than required to produce significantly enhanced light absorption due to the near-field plasmonic effect.[8] However, we have observed an increase of cell performance by modification of the interfacial properties.[22] Light scattering is also a way in which light harvesting can be improved because of the light-trapping

Received: May 24, 2018
Accepted: August 9, 2018
Published: August 23, 2018

Downloaded via UNIV JAUME I on February 12, 2019 at 08:37:40 (UTC).
See https://pubs.acs.org/sharingguidelines for options on how to legitimately share published articles.

© 2018 American Chemical Society

DOI: 10.1021/acsomega.8b01119
ACS Omega 2018, 3, 9798−9804

enhancement. Nanopatterned mp-TiO_2 layers enhance the light-harvesting efficiency of PSCs.[23] In addition, the high scattering efficiency observed for big Au/SiO_2 NPs demonstrates to be an effective way of improving light harvesting because of the redirection of the incident light into solar cells with increased optical path lengths (light-trapping effect).[24−27] In terms of material preparation process and cost, the total elimination of Au can be highly interesting if SiO_2 dielectric NPs could also induce a beneficial role on PSCs. The use of a mesoporous layer of SiO_2 instead of the conventional TiO_2 has been investigated.[28] However, the record performance for PSCs has always been reported with a TiO_2 mesoporous layer.[7−11] Here, we propose further enhancement of the TiO_2 mesoporous scaffold by the introduction of SiO_2 NPs on it.

In this study, we synthesized SiO_2 NPs, incorporating them within the mesoporous TiO_2 layer to fabricate PSCs. The cell structure was fluorine-doped tin oxide (FTO)/compact TiO_2/TiO_2 mesoporous containing SiO_2/$CH_3NH_3PbI_3$/spiro-OMeTAD/Au (Figure 1). Two different sizes of SiO_2 NPs, 50 and 100 nm, and different concentrations within the mesoporous layer were tested to exploit the effect of these NPs in the solar cell performance.

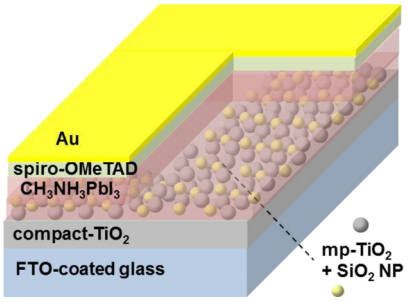

Figure 1. Schematic of the PSC structure where the TiO_2 mesoporous layer is modified with SiO_2 NPs. Compact TiO_2 and spiro-OMeTAD as electron and hole selective contacts, respectively.

2. EXPERIMENTAL PROCEDURE

2.1. Synthesis of SiO_2 NPs. The sol−gel method was used for the synthesis of SiO_2 NPs with diameters of 50 and 100 nm by hydrolyzing tetraethylorthosilicate (TEOS) in a mixture of ethanol, water, ammonia, and a surfactant. TEOS, ethanol, and ammonia were used as the silica precursor, the common solvent, and the catalyst, respectively. Typically, 5.5 mL of ethanol, 11 mL of deionized water, and 0.8 mL of ammonia were mixed and stirred at 30 °C (for 100 nm SiO_2 NPs) or 40 °C (for 50 nm SiO_2 NPs). At the same time, a solution containing 5.5 mL of ethanol and 1.7 mL of TEOS was prepared and stirred at 30 °C (for 100 nm SiO_2 NPs) or 40 °C (for 50 nm SiO_2 NPs). Then, the latter was added to the first solution, and the reaction mixture was maintained at 30 or 40 °C (depending on the desired particle size) for 2 h. During this time, the reaction turned turbid slowly because of the formation of silica NPs. Once the reaction was completed, 3-amino-propyltriethoxysilane was added dropwise to stabilize the particles. The resulting solution was heated at 80−90 °C to remove the excess of ammonia. The precipitate was collected by centrifugation and washed several times with water and ethanol; then, it was dried overnight at 100 °C. Figures S1 and S2 show the transmission electron microscopy (TEM) images of the SiO_2 NPs with 50 and 100 nm sizes, respectively.

2.2. Cell Fabrication. PSCs were fabricated in a structure based on FTO glass substrates, which were partially etched using HCl and zinc powder, cleaned with soap and deionized water, sonicated in a mixture of acetone/ethanol and then in acetone/isopropyl alcohol, and dried with compressed air. The substrates were then treated by an ultraviolet−ozone lamp for 15 min. To prepare the TiO_2 blocking layer (bl-TiO_2),

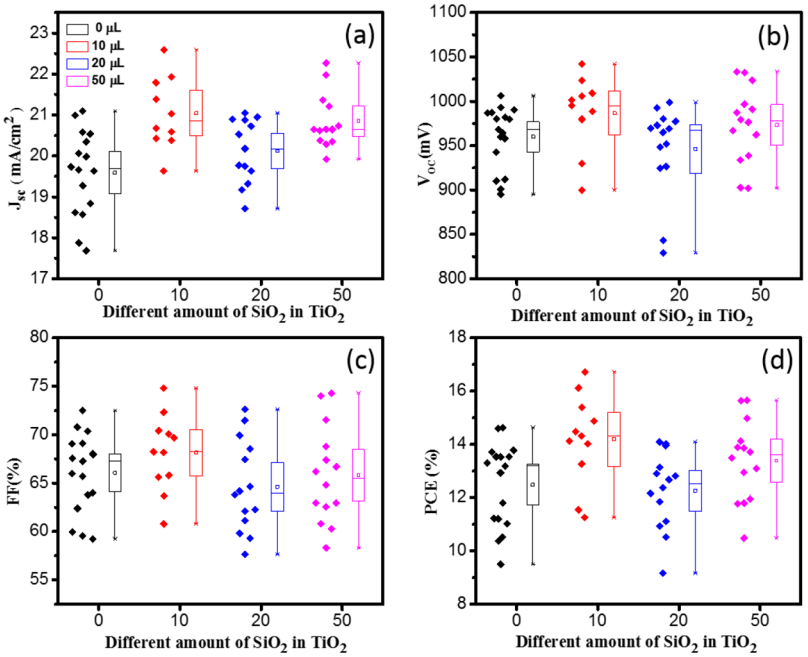

Figure 2. Boxplot showing the minimum, quartile 1, mean, median, quartile 3, and maximum for the photovoltaic performance of cells using different concentrations of SiO_2 NPs of 100 nm size. (a) J_{sc}, (b) V_{oc}, (c) FF, and (d) PCE. Concentration is indicated in μL of a solution of 0.4 mg of SiO_2 powder in 10 mL of ethanol.

DOI: 10.1021/acsomega.8b01119
ACS Omega 2018, 3, 9798−9804

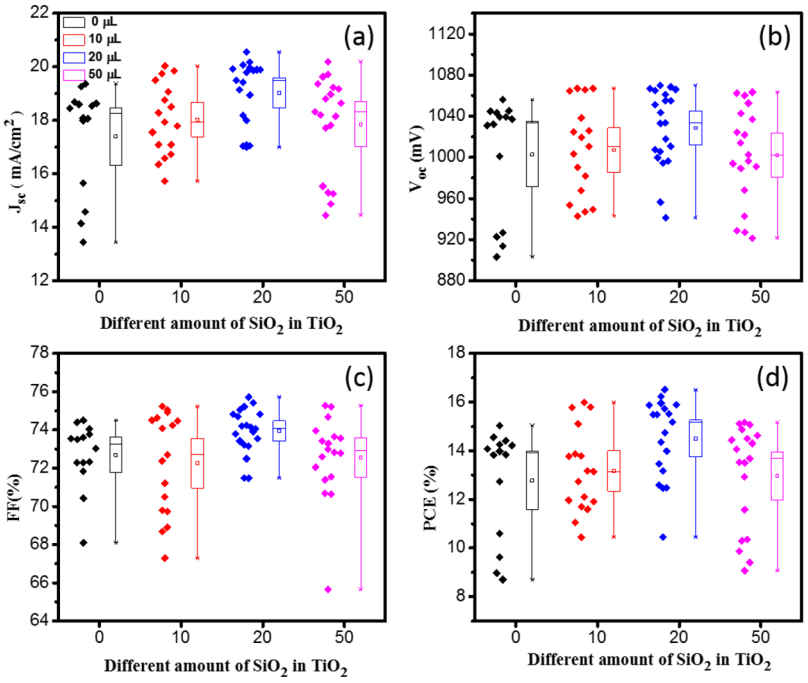

Figure 3. Boxplot showing the minimum, quartile 1, mean, median, quartile 3, and maximum for the photovoltaic performance of cells using different concentrations of SiO_2 NPs of 50 nm size. (a) J_{sc}, (b) V_{oc}, (c) FF, and (d) PCE. Concentration is indicated in μL of a solution of 0.4 mg of SiO_2 powder in 10 mL of ethanol.

titanium diisopropoxide dis(acetylacetonate) in ethanol (1:9, v/v) was deposited by spray pyrolysis at 450 °C, and then the film was annealed at 450 °C for 30 min in air. SiO_2 (0.4 mg) powder in 10 mL of ethanol was stirred for 1 night. Different concentrations of SiO_2 solution (0, 10, 20, and 50 μL) were combined with a dilute commercial TiO_2 paste (30NRT) in ethanol (1:5 weight ratio). Then, the SiO_2/TiO_2 (mp-TiO_2) layer was deposited on the bl-TiO_2 layer by spin-coating at 2000 rpm for 10 s. After drying at 100 lC for 10 min, it was annealed in air up to 500 aC for 30 min. Lithium bis-(strifluoromethanesulfonamide) (Li-TFSI, 35 mM) solution in acetonitrile was deposited on the substrates by spin-coating at 3000 rpm for 10 s. This Li-TFSI deposition has been performed for samples using SiO_2 with 50 nm, but not for 100 nm, to rule out the influence of treatment instead of NP incorporation. Then, the substrates were annealed at 450 PC for 30 min.[29] PbI_2 (622 mg) and 105 mg of dimethyl sulfoxide were mixed in 944 mg of dimethylformamide (DMF) solution inside a glovebox. This solution was heated at 65 oC and then mixed into 214 mg of CH_3NH_3I. The completely dissolved solution was spin-coated on the substrate layer at 4000 rpm for 50 s. Also, on the rotating substrate, diethyl ether was dripped, which caused rapid vaporization of DMF. Then, the deposited film was heated at 100 wC to obtain a dense $CH_3NH_3PbI_3$ film. Then, 72.3 mg of spiro-OMeTAD, 28.8 μL of 4-*tert*-butyl pyridine, and 17.5 μL of Li-TFSI solution (520 mg/mL of Li-TFSI in acetonitrile) were dissolved in 1 mL of chlorobenzene and deposited on the perovskite layer as a hole-transfer layer by spin-coating at 4000 rpm for 30 s. Finally, the electrode contacts (60 nm Au) were deposited on the cells by thermal evaporation in a high vacuum chamber.

2.3. Characterization. The current−voltage (J−V) curves were obtained with a scan rate of 50 mV/s in an Abet Technologies Sun 2000 Class A AM 1.5G solar simulator with a Keithley 2612 Source Meter, where the light intensity was adjusted with an NREL-calibrated Si solar cell with a KG-5 filter to 1 sun of intensity (100 mW/cm^2) in the Institute of Advanced Materials (INAM) at Universitat Jaume I. The measurements were performed using a shadow mask with an area of 0.101 cm^2. Ultraviolet−visible absorption spectra were recorded by using a Cary 500 Scan VARIAN spectrophotometer in the 250−800 nm wavelength range. Impedance spectroscopy measurements were performed using an Autolab PGSTAT-30 instrument equipped with a frequency analyzer module at 0.1 sun light illumination. The dc bias was selected at 0 V, and the ac perturbation was 60 mV covering the frequency range of 0.1 Hz to 1 MHz. The integration time was 0.125 s, and the number of cycles was equal to one.

3. RESULTS AND DISCUSSION

To demonstrate the effect of SiO_2 NPs on the PSC performance, the fabricated cells were tested (with different concentrations and sizes of SiO_2) under 1 sun condition in air. Figures 2 and 3 show the dependence of the average device performance parameters when the concentration of SiO_2 NPs, with 100 and 50 nm sizes, respectively, varies from 0 to 10 and 50 μL. To ensure reliability, at least 15 devices were made for each concentration, but usually more devices are prepared in a single condition. We have analyzed several batches at each condition, and two operators prepared the devices to avoid dispersion from batch to batch, independent of the skill of a single operator. No cell was ruled out of the analysis despite some batches presenting a significant lower performance than the average. This procedure implies the preparation of a large amount of samples, as we have prepared in this work, to have a confidence interval as high as 90%, where no overlap is observed between the intervals for the samples having the highest PCE and the reference, as we show in Figures S3 and S4, making the study statistically meaningful. The boxplot featuring the short-circuit current density (J_{sc}), open circuit

DOI: 10.1021/acsomega.8b01119
ACS Omega 2018, 3, 9798−9804

potential (V_{oc}), fill factor (FF), and PCE of all of the cells with different SiO_2 NP concentrations are compared in Figures 2 and 3. Clearly, the addition of SiO_2 NPs demonstrates an increase in the J_{sc} and hence in the PCE. In particular, the highest PCE for samples containing 50 and 100 nm size SiO_2 NPs embedded in the TiO_2 mesoporous scaffold was achieved by using 20 and 10 μL solutions, respectively. No significant variation in light absorbance was observed after the addition of SiO_2 NPs, see Figure S5.

The values of the photovoltaic parameters for the cells with the highest PCE with different SiO_2 NP concentrations and sizes are summarized in Table 1. Again, the cells with NPs exhibit higher photovoltaic parameters. Clearly, the observed PCE enhancement for the device incorporating SiO_2 NPs mainly comes from the great improvement of J_{sc} because the V_{oc} and FF exhibit only a slight change. The maximum PCE of the devices without NPs reaches 15.04%, whereas the maximum PCE of those incorporating the NPs reaches 16.51 and 16.71% for sizes of 50 and 100 nm, respectively. The $J-V$ curves of these champion cells are plotted in Figure S6.

Table 1. Values of J_{sc}, V_{oc}, FF, and PCE for Champion PSCs with Different Concentrations and Sizes of SiO_2 NPs under the Irradiation of 1 sun Intensity (100 mW/cm^2; AM 1.5G)

size (nm)	SiO_2 (μL)	J_{sc} (mA/cm^2)	V_{oc} (V)	FF (%)	PCE (%)
50	0	19.35	1.055	73	15.04
	10	20.03	1.065	74	15.99
	20	20.55	1.061	75	16.51
	50	19.72	1.052	72	15.15
100	0	20.06	1.006	72.47	14.63
	10	22.59	1.023	72.32	16.71
	20	20.17	0.998	69.94	14.09
	50	20.38	1.033	74.29	15.64

To highlight the cause of the observed enhancement of PCE performance, the optical properties of the mesoporous scaffold have been theoretically analyzed to calculate the effect of incorporation of SiO_2 NPs of different sizes. The obtained results are consistent with the scattering of SiO_2 NPs inside the TiO_2 scaffold calculated by the Mie theory.[30] First, the scattering cross-section ($\sigma_{scattering}$) of a SiO_2 NP immersed in the TiO_2 bulk matrix induces a clear scattering enhancement by increasing the size (radius) of the NP, as illustrated in Figure 4a. This behavior agrees with previous calculations carried out with metal NPs in polymer media[15] and can qualitatively explain the enhancement of the solar cell efficiency when 100 nm size SiO_2 NPs are used inside the TiO_2 scaffold. Moreover, the dependence of the scattering as a function of the filling factor (FF, volume of SiO_2 inside the TiO_2 matrix) will exhibit an optimum concentration, as presented in Figure 4b for a size of 100 nm. Here, it was important to take into account the mesoporous nature of TiO_2: it seems that for low concentrations, SiO_2 is totally covered by TiO_2, whereas for a high FF, the NPs "can see" the influence of the air present in the porous layer, and an effective index medium has to be considered.[15] Under these conditions, $\sigma_{scattering}$ decreases for large concentrations, where the effective refractive index of the matrix will approach that of SiO_2. Nevertheless, because the total scattering is proportional to the number of NPs (and hence, FF), there is an optimum concentration that maximizes the scattering of light and, with it, the efficiency of the solar cell (see Figure 4b). In addition, other effects such as the improvement of the contact between the perovskite and the mesoporous layer by the presence of large size SiO_2 NPs can also contribute for enhancing the PSC performance.

On the other hand, the enhancement on cell performance observed when 100 nm NPs are used instead of 50 nm NPs is significantly more moderate than that expected from the theoretical analysis, as highlighted in Figure 4a. Here, it is worthy to note that the thickness of the scaffold, ~200 nm, is of the same order as the SiO_2 NP size, and consequently an excessive increase of the NP concentration would affect seriously the morphology of this layer and even light transmission, effects that were not considered in Figure 4.

The PCE enhancement achieved, according to Table 1, was 9 and 14% for NPs 50 and 100 nm in diameter, respectively, which can be explained as a consequence of the light-trapping effect of the NPs. These NPs act like mirrors inside of the mesoporous layer; the sunlight is scattered on it, enabling a longer optical path length, and thereby a higher amount of light is absorbed by the perovskite. One of the most interesting characteristics of the method proposed here to enhance the PCE is the fact that this TiO_2–SiO_2 nanocomposite is obtained through a simple mixing step, indicating the feasibility of the proposed method easily upscalable. There are other light-trapping mechanisms, as nanotextures,[31] that theoretically can achieve a higher enhancement, but require a complicated fabrication method that is difficult to transfer to industrial applications.

It is well-known that the mesoporous scaffold also plays an important role in the recombination and decrease of hysteresis.[8,32] In addition to the increase of PCE with the incorporation of SiO_2, a significant decrease in the $J-V$ hysteresis is observed, see Figure 5 and Table 2. The forward

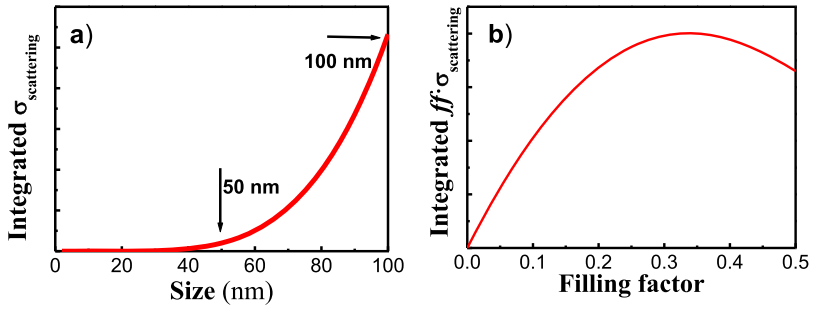

Figure 4. (a) Integrated scattering cross-section as a function of the size of the SiO_2 NP inside the TiO_2 matrix. (b) Integrated scattering cross-section per FF as a function of FF. Size was fixed to 100 nm.

DOI: 10.1021/acsomega.8b01119
ACS Omega 2018, 3, 9798–9804

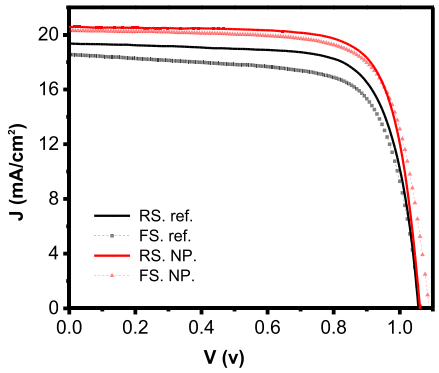

Figure 5. $J-V$ hysteresis of champion PSCs with SiO_2 NPs (50 nm) and without NPs (ref.). RS, reverse scan from V_{oc} to zero. FS, forward scan from zero to V_{oc}.

Table 2. Hysteresis Factor Extracted from the Data Using the Definition Provided in Eq 1

SiO_2 (μL)	0	10	20	30
HI	0.102	0.032	0.018	0.024

and reverse sweeps of the $J-V$ curve for reference devices with no SiO_2 and for devices with SiO_2 NPs of 50 nm are summarized in Table S1. The hysteresis index (HI) has been quantified by calculating as follows[33]

$$\mathrm{HI} = \frac{J_{\mathrm{Rev}}\left(\frac{V_{oc}}{2}\right) - J_{\mathrm{For}}\left(\frac{V_{oc}}{2}\right)}{J_{\mathrm{Rev}}\left(\frac{V_{oc}}{2}\right)} \quad (1)$$

where $J_{\mathrm{Rev}}(V_{oc}/2)$ and $J_{\mathrm{For}}(V_{oc}/2)$ are the currents when half of the V_{oc} voltage is applied for reverse (from V_{oc} to zero) and forward (from zero to V_{oc}) voltage scans, respectively. A HI of 0 corresponds to a cell without significant hysteresis, whereas a HI of 1 corresponds to a system in which the hysteresis is as high as the photocurrent.

Different aspects contribute to hysteresis in PSCs, among them, ion migration and accumulation at perovskite interfaces is one of the most influencing ones.[34] One easy way to weigh the effect of ion accumulation is by open circuit voltage decay (OCVD) measurements.[35] Light soaking produces an accumulation of ions at the interface. This charge accumulation causes an electrostatic potential adding its value to the built-in potential from the V_{oc}. After switching off the illumination in OCVD measurements, two regimes are observed. First, a fast decrease is observed as the built-in potential induced by carrier photogeneration is quickly removed. For longer times, a significantly slower decay is observed as the elimination of the electrostatic potential is related with the slow ion migration that removes the ion accumulation. OCVD measurements for PSCs with and without SiO_2 NPs are plotted in Figure 6. Although both kinds of samples present the same behavior in the fast decay regime, a clear difference is observed in the slow decay regime. Samples with SiO_2 NPs are able to remove the electrostatic potential induced by ion accumulation faster than reference cells, pointing to a lower ion accumulation and/or a faster dynamic in samples with SiO_2 NPs. In this sense, the addition of SiO_2 NPs is not just affecting the optical properties of the mesoporous scaffold but also affecting the ion migration properties of the perovskite deposited in it. Alternatively, ion accumulation was also monitored by the low-frequency capacitance.[32,36−38] Samples with SiO_2 NPs present lower

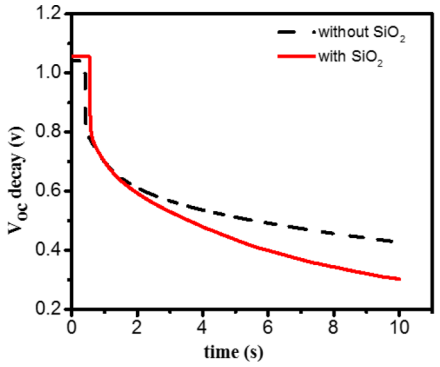

Figure 6. OCVD for cells with and without NPs (50 nm SiO_2).

low-frequency capacitance, see Figure S7, pointing to a lower ion accumulation in good agreement with the OCVD measurements.

4. CONCLUSIONS

SiO_2 NPs with 50 and 100 nm sizes have been integrated into a conventional mesoporous TiO_2 layer of the PSCs, observing an enhancement of cell performance up to 14%, in comparison with reference samples, mainly because of an increase in the photocurrent. These results are in good agreement with the theoretical predictions based on the increase of light scattering induced by the presence of SiO_2. Light scattering is favored by the increase of the NP size. However, as the size that is able to produce significant scattering is comparable with the optimum mesoporous layer thickness, other aspects such as the layer morphology, the loss in transparency, and the reduction of the effective refractive index have to be properly balanced to optimize the SiO_2 concentration in the mesoporous scaffold. The addition of SiO_2 NPs also affects the ion accumulation at the perovskite interfaces, causing an additional beneficial effect, reducing the cell hysteresis significantly. Here, we show a method, easy to implement, to increase the PSC performance by the modification of the mesoporous TiO_2 scaffold with the addition of dielectric SiO_2 NPs, pointing concretely to the development of new mesoporous layers as a way to further increase the performance of PSCs. Optimization of optical properties has allowed the latest improvement in performance in very high-efficient GaAs solar cells and has to be necessarily considered as the reported efficiency of the photovoltaic technology is approaching the Shockley−Queisser limit, as it is the case for PSCs.

■ ASSOCIATED CONTENT

Supporting Information

The Supporting Information is available free of charge on the ACS Publications website at DOI: 10.1021/acsomega.8b01119.

Size histogram and TEM image of SiO_2 NPs with 50 and 100 nm average sizes, $J-V$ curves of champion cells, and average solar cell parameters measured with FS and RS for different SiO_2 concentrations (PDF)

■ AUTHOR INFORMATION

Corresponding Author

*E-mail: sero@uji.es.

ORCID

Isaac Suarez: 0000-0002-2773-8801

DOI: 10.1021/acsomega.8b01119
ACS Omega 2018, 3, 9798−9804

Pablo Ortiz: 0000-0002-1049-4409
Ivan Mora-Seró: 0000-0003-2508-0994

Notes

The authors declare no competing financial interest.

■ ACKNOWLEDGMENTS

N.A. thanks the Iranian Ministry of Science and Technology (Tehran, Iran) and the Yazd University for supporting her visit to the Institute of Advanced Materials (INAM) at Universitat Jaume I (Spain). The work was supported by the European Research Council (ERC) via Consolidator Grant (724424—No-LIMIT) by MINECO of Spain (projects MAT2013-47192-C3-1-R and TEC2017-86102-C2-1-R) and by Generalitat Valenciana (projects PROMETEOII/2014/020 and PROMETEOII/2014/059).

■ REFERENCES

(1) Im, J.-H.; Lee, C.-R.; Lee, J.-W.; Park, S.-W.; Park, N.-G. 6.5% efficient perovskite quantum-dot-sensitized solar cell. *Nanoscale* **2011**, *3*, 4088−4093.
(2) Kojima, A.; Teshima, K.; Shirai, Y.; Miyasaka, T. Organometal Halide Perovskites as Visible-Light Sensitizers for Photovoltaic Cells. *J. Am. Chem. Soc.* **2009**, *131*, 6050−6051.
(3) Kim, H.-S.; Lee, C.-R.; Im, J.-H.; Lee, K.-B.; Moehl, T.; Marchioro, A.; Moon, S.-J.; Humphry-Baker, R.; Yum, J.-H.; Moser, J. E.; Grätzel, M.; Park, N.-G. Lead Iodide Perovskite Sensitized All-Solid-State Submicron Thin Film Mesoscopic Solar Cell with Efficiency Exceeding 9%. *Sci. Rep.* **2012**, *2*, 591.
(4) Lee, M. M.; Teuscher, J.; Miyasaka, T.; Murakami, T. N.; Snaith, H. J. Efficient Hybrid Solar Cells Based on Meso-Superstructured Organometal Halide Perovskites. *Science* **2012**, *338*, 643−647.
(5) Aharon, S.; Cohen, B. E.; Etgar, L. Hybrid Lead Halide Iodide and Lead Halide Bromide in Efficient Hole Conductor Free Perovskite Solar Cell. *J. Phys. Chem. C* **2014**, *118*, 17160−17165.
(6) Yang, W. S.; Park, B.-W.; Jung, E. H.; Jeon, N. J.; Kim, Y. C.; Lee, D. U.; Shin, S. S.; Seo, J.; Kim, E. K.; Noh, J. H.; Seok, S. I. Iodide management in formamidinium-lead-halide-based perovskite layers for efficient solar cells. *Science* **2017**, *356*, 1376−1379.
(7) Burschka, J.; Pellet, N.; Moon, S.-J.; Humphry-Baker, R.; Gao, P.; Nazeeruddin, M. K.; Grätzel, M. Sequential deposition as a route to high-performance perovskite-sensitized solar cells. *Nature* **2013**, *499*, 316−319.
(8) Jeon, N. J.; Noh, J. H.; Kim, Y. C.; Yang, W. S.; Ryu, S.; Seok, S. I. Solvent engineering for high-performance inorganic−organic hybrid perovskite solar cells. *Nat. Mater.* **2014**, *13*, 897−903.
(9) Jeon, N. J.; Noh, J. H.; Yang, W. S.; Kim, Y. C.; Ryu, S.; Seo, J.; Seok, S. I. Compositional engineering of perovskite materials for high-performance solar cells. *Nature* **2015**, *517*, 476−480.
(10) Saliba, M.; Matsui, T.; Seo, J.-Y.; Domanski, K.; Correa-Baena, J.-P.; Nazeeruddin, M. K.; Zakeeruddin, S. M.; Tress, W.; Abate, A.; Hagfeldt, A.; Grätzel, M. Cesium-containing triple cation perovskite solar cells: improved stability, reproducibility and high efficiency. *Energy Environ. Sci.* **2016**, *9*, 1989−1997.
(11) Yang, W. S.; Noh, J. H.; Jeon, N. J.; Kim, Y. C.; Ryu, S.; Seo, J.; Seok, S. I. High-performance photovoltaic perovskite layers fabricated through intramolecular exchange. *Science* **2015**, *348*, 1234−1237.
(12) Gangishetty, M. K.; Lee, K. E.; Scott, R. W. J.; Kelly, T. L. Plasmonic Enhancement of Dye Sensitized Solar Cells in the Red-to-near-Infrared Region using Triangular Core−Shell Ag@SiO2 Nanoparticles. *ACS Appl. Mater. Interfaces* **2013**, *5*, 11044−11051.
(13) Huang, F.; Chen, D.; Zhang, X. L.; Caruso, R. A.; Cheng, Y.-B. Dual-Function Scattering Layer of Submicrometer-Sized Mesoporous TiO2Beads for High-Efficiency Dye-Sensitized Solar Cells. *Adv. Funct. Mater.* **2010**, *20*, 1301−1305.
(14) Balraju, P.; Suresh, P.; Kumar, M.; Roy, M. S.; Sharma, G. D. Effect of counter electrode, thickness and sintering temperature of TiO2 electrode and TBP addition in electrolyte on photovoltaic performance of dye sensitized solar cell using pyronine G (PYR) dye. *J. Photochem. Photobiol., A* **2009**, *206*, 53−63.
(15) Signoretto, M.; Suárez, I.; Chirvony, V. S.; Abargues, R.; Rodríguez-Cantó, P. J.; Martínez-Pastor, J. Polymer waveguide couplers based on metal nanoparticle-polymer nanocomposites. *Nanotechnology* **2015**, *26*, 475201.
(16) Lu, Z.; Pan, X.; Ma, Y.; Li, Y.; Zheng, L.; Zhang, D.; Xu, Q.; Chen, Z.; Wang, S.; Qu, B.; Liu, F.; Huang, Y.; Xiao, L.; Gong, Q. Plasmonic-enhanced perovskite solar cells using alloy popcorn nanoparticles. *RSC Adv.* **2015**, *5*, 11175−11179.
(17) Saliba, M.; Zhang, W.; Burlakov, V. M.; Stranks, S. D.; Sun, Y.; Ball, J. M.; Johnston, M. B.; Goriely, A.; Wiesner, U.; Snaith, H. J. Plasmonic-Induced Photon Recycling in Metal Halide Perovskite Solar Cells. *Adv. Funct. Mater.* **2015**, *25*, 5038−5046.
(18) Zhang, W.; Saliba, M.; Stranks, S. D.; Sun, Y.; Shi, X.; Wiesner, U.; Snaith, H. J. Enhancement of Perovskite-Based Solar Cells Employing Core−Shell Metal Nanoparticles. *Nano Lett.* **2013**, *13*, 4505−4510.
(19) Carretero-Palacios, S.; Jiménez-Solano, A.; Míguez, H. Plasmonic Nanoparticles as Light-Harvesting Enhancers in Perovskite Solar Cells: A User's Guide. *ACS Energy Lett.* **2016**, *1*, 323−331.
(20) Arinze, E. S.; Qiu, B.; Nyirjesy, G.; Thon, S. M. Plasmonic Nanoparticle Enhancement of Solution-Processed Solar Cells: Practical Limits and Opportunities. *ACS Photonics* **2016**, *3*, 158−173.
(21) Pathak, N. K.; Chander, N.; Komarala, V. K.; Sharma, R. P. Plasmonic Perovskite Solar Cells Utilizing Au@SiO2 Core-Shell Nanoparticles. *Plasmonics* **2017**, *12*, 237−244.
(22) Aeineh, N.; Barea, E. M.; Behjat, A.; Sharifi, N.; Mora-Seró, I. Inorganic Surface Engineering to Enhance Perovskite Solar Cell Efficiency. *ACS Appl. Mater. Interfaces* **2017**, *9*, 13181−13187.
(23) Kang, S. M.; Jang, S.; Lee, J.-K.; Yoon, J.; Yoo, D.-E.; Lee, J.-W.; Choi, M.; Park, N.-G. Moth-Eye TiO2 Layer for Improving Light Harvesting Efficiency in Perovskite Solar Cells. *Small* **2016**, *12*, 2443−2449.
(24) Atwater, H. A.; Polman, A. Plasmonics for improved photovoltaic devices. *Nat. Mater.* **2010**, *9*, 205−213.
(25) Cai, B.; Peng, Y.; Cheng, Y.-B.; Gu, M. 4-fold photocurrent enhancement in ultrathin nanoplasmonic perovskite solar cells. *Opt. Express* **2015**, *23*, A1700−A1706.
(26) Koo, H.-J.; Kim, Y. J.; Lee, Y. H.; Lee, W. I.; Kim, K.; Park, N.-G. Nano-embossed Hollow Spherical TiO2 as Bifunctional Material for High-Efficiency Dye-Sensitized Solar Cells. *Adv. Mater.* **2008**, *20*, 195−199.
(27) Koo, H.-J.; Park, J.; Yoo, B.; Yoo, K.; Kim, K.; Park, N.-G. Size-dependent scattering efficiency in dye-sensitized solar cell. *Inorg. Chim. Acta* **2008**, *361*, 677−683.
(28) Hwang, S. H.; Roh, J.; Lee, J.; Ryu, J.; Yun, J.; Jang, J. Size-controlled SiO2 nanoparticles as scaffold Layers in thin-film perovskite solar cells. *J. Mater. Chem. A* **2014**, *2*, 16429−16433.
(29) Giordano, F.; Abate, A.; Baena, J. P. C.; Saliba, M.; Matsui, T.; Im, S. H.; Zakeeruddin, S. M.; Nazeeruddin, M. K.; Hagfeldt, A.; Graetzel, M. Enhanced electronic properties in mesoporous TiO2 via lithium doping for high-efficiency perovskite solar cells. *Nat. Commun.* **2016**, *7*, 10379.
(30) Myroshnychenko, V.; Rodríguez-Fernández, J.; Pastoriza-Santos, I.; Funston, A. M.; Novo, C.; Mulvaney, P.; Liz-Marzán, L. M.; de Abajo, F. J. G. Modelling the optical response of gold nanoparticles. *Chem. Soc. Rev.* **2008**, *37*, 1792−1805.
(31) Xie, Z.; Sun, S.; Wang, W.; Qin, L.; Yan, Y.; Hou, R.; Qin, G. G. Simulation study on improving efficiencies of perovskite solar cell: Introducing nano textures on it. *Opt. Commun.* **2018**, *410*, 117−122.
(32) Anaya, M.; Zhang, W.; Hames, B. C.; Li, Y.; Fabregat-Santiago, F.; Calvo, M. E.; Snaith, H. J.; Míguez, H.; Mora-Seró, I. Electron injection and scaffold effects in perovskite solar cells. *J. Mater. Chem. C* **2017**, *5*, 634−644.
(33) Sanchez, R. S.; Gonzalez-Pedro, V.; Lee, J.-W.; Park, N.-G.; Kang, Y. S.; Mora-Sero, I.; Bisquert, J. Slow Dynamic Processes in Lead Halide Perovskite Solar Cells. Characteristic Times and Hysteresis. *Chem. Phys. Lett.* **2014**, *5*, 2357−2363.

DOI: 10.1021/acsomega.8b01119
ACS Omega 2018, 3, 9798−9804

(34) Chen, B.; Yang, M.; Priya, S.; Zhu, K. Origin of J−V Hysteresis in Perovskite Solar Cells. *J. Phys. Chem. Lett.* **2016**, *7*, 905−917.
(35) Gottesman, R.; Lopez-Varo, P.; Gouda, L.; Jimenez-Tejada, J. A.; Hu, J.; Tirosh, S.; Zaban, A.; Bisquert, J. Dynamic Phenomena at Perovskite/Electron-Selective Contact Interface as Interpreted from Photovoltage Decays. *Chem* **2016**, *1*, 776−789.
(36) Kim, H.-S.; Jang, I.-H.; Ahn, N.; Choi, M.; Guerrero, A.; Bisquert, J.; Park, N.-G. Control of I−V Hysteresis in CH3NH3PbI3 Perovskite Solar Cell. *J. Phys. Chem. Lett.* **2015**, *6*, 4633−4639.
(37) Zarazua, I.; Bisquert, J.; Garcia-Belmonte, G. Light-Induced Space-Charge Accumulation Zone as Photovoltaic Mechanism in Perovskite Solar Cells. *J. Phys. Chem. Lett.* **2016**, *7*, 525−528.
(38) Zarazua, I.; Han, G.; Boix, P. P.; Mhaisalkar, S.; Fabregat-Santiago, F.; Mora-Seró, I.; Bisquert, J.; Garcia-Belmonte, G. Surface Recombination and Collection Efficiency in Perovskite Solar Cells from Impedance Analysis. *J. Phys. Chem. Lett.* **2016**, *7*, 5105−5113.

DOI: 10.1021/acsomega.8b01119
ACS Omega 2018, 3, 9798−9804